THE JOURNAL OF PHYSICAL CHEMISTRY B

Article

pubs.acs.org/JPCB

Introduction of a Hydrogen Bond between Phylloquinone PhQ_A and a Threonine Side-Chain OH Group in Photosystem I

Sam Mula,[†] Michael D. McConnell,[‡] Amy Ching,[†] Nan Zhao,[§] Heather L. Gordon,[†] Gary Hastings,[§] Kevin E. Redding,*[,‡] and Art van der Est*[,†]

[†]Department of Chemistry, Brock University, St. Catharines, Ontario, Canada

[‡]Department of Chemistry and Biochemistry, Arizona State University, Tempe, Arizona, United States

[§]Department of Physics and Astronomy, Georgia State University, Atlanta, Georgia, United States

ABSTRACT: The phylloquinone acceptor PhQ_A in photosystem I binds to the protein through a single H-bond to the backbone nitrogen of PsaA-L722. Here, we investigate the effect of this H-bond on the electron transfer (ET) kinetics by substituting threonine for PsaA-L722. Room temperature spin-polarized transient EPR measurements show that in the PsaA-L722T mutant, the rate of PhQ_A^- to F_X ET increases and the hyperfine coupling to the 2-methyl group of PhQ_A is much larger than in the wild type. Molecular dynamics simulations and ONIOM type electronic structure calculations indicate that it is possible for the OH group of the Thr side chain to form an H-bond to the carbonyl oxygen atom, O_4 of the phylloquinone, and that this results in an increase in the 2-methyl hyperfine couplings as observed in the transient EPR data. The Arrhenius plot of the PhQ_A^- to F_X ET in the PsaA-L722T mutant suggests that the increased rate is probably the result of a slight change in the electronic coupling between PhQ_A^- and F_X. The strong deviation from Arrhenius behavior observed at ~200 K can be reproduced using a semiclassical model, which takes the zero-point energy of the mode coupled to the ET into account. However, since the change in slope of the Arrhenius plot occurs at the protein glass transition temperature, it is argued that it could be the result of a change in the protein relaxation dynamics at this temperature rather than quantum mechanical effects.

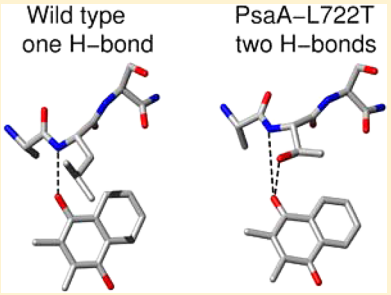

INTRODUCTION

In oxygenic photosynthesis, photosystem I (PS I) uses light to transfer electrons from plastocyanin on the lumenal side of the thylakoid membrane to ferredoxin on the stromal side.[1] The electron transport chain consists of two branches of cofactors that diverge at the chlorophyll *a*/*a*′ dimer, P_{700}, on the donor side and converge again at F_X, the first of three 4Fe-4S iron–sulfur clusters on the acceptor side. The two branches are labeled A and B according to which protein subunit, PsaA or PsaB, provides the majority of the bonds to the cofactors[2] and each of them contains two chlorophyll *a* molecules, ec2 and ec3, and a phylloquinone, PhQ. There is some variability in the side chains of the phylloquinones between species but the headgroup is the same.[3] The acceptor side of the complex is strongly reducing and the two phylloquinone acceptor molecules have unusually low midpoint potentials in the vincinity of −800 mV,[4] which is ~350 mV more negative than in aprotic solvent.[5] Although it is clear that the phylloquinone binding pocket plays an important role in shifting the quinone potentials to more negative values, many details of how this occurs are uncertain. More importantly, the relationship between the structure of the binding pocket, the midpoint potential of the quinone and the rate of electron transfer (ET) is not well understood. As can be seen in the X-ray structure[6,7] of the PhQ_A phylloquinone binding site (Figure 1), one of the two carbonyl oxygen atoms of the quinone headgroup is hydrogen bonded to the backbone nitrogen of PsaA-L722.[6,7]

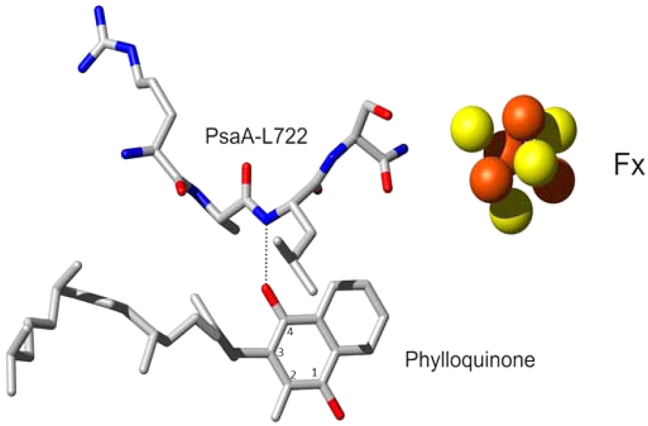

Figure 1. A-Branch phylloquinone binding site in PS I from the 2.5-Å resolution X-ray crystal structure (PDB code: 1JB0).[6,7] The figure was constructed using the program MOLMOL.[8].

The role of this H-bond has been investigated recently[9−12] using point mutations to selectively alter residue PsaA-722 or the corresponding B-branch residue PsaB-706. It was shown that replacement of PsaA-L722 with a bulky tryptophan leads

Received: September 21, 2012
Revised: November 7, 2012

   dx.doi.org/10.1021/jp309410w | *J. Phys. Chem. B* XXXX, XXX, XXX−XXX

to changes in the spin density distribution on the semiquinone headgroup consistent with weakening or loss of the H-bond.[10] Such a change would be expected to destabilize the semiquinone and consistent with this expectation, the rate of ET from PhQ_A to F_X increased in the PsaA-L722W mutant.[11] It was proposed that the larger size of the tryptophan side chain compared to that of leucine likely forces a rearrangement of the protein such that the backbone N of reside PsaA-722 moves away from the phylloquinone and breaks or weakens the H-bond. Tyrosine and threonine mutants of PsaA-L722 have also been constructed and were used as part of a study to investigate interquinone ET.[12] Both the PsaA-L722Y and PsaA-L722T mutants showed shorter lifetimes for PhQ_A to F_X ET, but the effect of the mutations on the phylloquinone H-bonding was not investigated. In the case of the PsaA-L722Y mutant, the faster ET is expected because the tyrosine side chain is also considerably larger than that of leucine, hence, the steric bulk suggested to cause breaking of the H-bond in the PsaA-L722W mutant should cause similar effects. However, the faster ET observed for the PsaA-L722T mutant is not as easy to rationalize because the side chain of threonine is smaller than that of leucine and, hence, breaking of the H-bond due to steric constraints seems unlikely. Moreover, threonine is polar and might be expected to cause some stabilization of the charge on the semiquinone, which would slow forward ET.

Here, we use transient EPR spectroscopy, quantum chemical calculations, and molecular dynamics simulations to investigate the effect of the incorporated threonine residue in the PsaA-L722T mutant on hydrogen bonding between PhQ_A and its binding site and on the ET kinetics. The results strongly suggest that PhQ_A is H-bonded to the OH group of the threonine side chain. The change in the H-bonding is expected to cause a shift of the quinone midpoint potential to a more positive value and should decrease the rate of forward ET. However, the observed rate of ET is faster than in the wild type. We argue that this is probably the result of a change in the electronic coupling between PhQ_A and F_X.

MATERIALS AND METHODS

Construction and Growth of the PsaA-L722T Mutant Strain. The PsaA-L722T mutation was created as described previously.[12,13] Briefly, a one-tube PCR method for site-directed mutagenesis was performed[14] using plasmids containing the *psaA*-3 exon and the *aadA*, antibiotic resistance gene. Mutant plasmids were delieved via biolistic bombardment into a *psaA*-3Δ strain (KCR1001-11A) of *Chlamydomonas reinhardtii*. Cells were grown under continuous low-light (10 μE $m^{-2}s^{-1}$) at room temperature on standard TAP media and were selected for resistance to spectinomycin and streptomycin.

Isolation of Photosystem I from the PsaA-L722T Mutant Strain. Cells were harvested and broken in a chilled French press at 3000 psi. Thylakoid membranes were solubilized on ice in darkness with 0.9% (wt/vol) *n*-dodecyl-β-D-maltoside at 0.8−1.0 mg·mL^{-1} Chl for 20 min, and the solubilized fraction was then isolated from the unsoluable debris by ultracentrifugation at 65000 g for 25 min. Solubilized membrane proteins were laid on sucrose density gradients, which were formed by the freeze−thaw, method and contained 5 mM tricine-NaOH (pH 8.0), 0.3 M sucrose, 0.3 M betaine, and 0.05% *n*-dodecyl-β-D-maltoside. Following a 20 h centrifugation at 120000 × *g*, the lowest green band was collected and concentrated in buffer containing 5 mM tricine-NaOH (pH 8.0), 5 mM $CaCl_2$, 5 mM $MgCl_2$, and 0.05% *n*-dodecyl-β-D-maltoside.[15]

Transient EPR Spectroscopy. Time/field transient EPR data sets were measured using a modified Bruker ER 200D-SRC spectrometer with either an ER 041 X-MR X-band or an ER 051 QR Q-band microwave bridge. For the X-band data sets, a Flexline ER 4118 X-MD-5W1 dielectric resonator was used at temperatures below 270 K and an ER 4103 TM rectangular resonator was employed at room temperature. An ER 5106 QT-W cylindrical resonator was used for the Q-band experiments. Light excitation was achieved using a Continuum Surelite Nd:YAG laser operating at 10 Hz, 4.0 mJ/pulse, and 532 nm. The temperature was controlled using an Oxford Instruments CF935 gas flow cryostat. The transient EPR signal was collected in direct-detection mode with a home-built broadband amplifier (bandwidth > 500 MHz) and was digitized using a LeCroy LT322 500 MHz digital oscilloscope and saved on a PC for analysis. Samples were treated with 1 mM sodium ascorbate and 50 μM phenazine methosulfate (PMS) and for the low temperature experiments, the samples were dark adapted for 20 min on ice and frozen in the dark to ensure complete reduction of P_{700}^+ before illumination.

Pulsed EPR Experiments. Out-of-phase echo modulation curves were collected at 80 K using a Bruker Elexsys E580 spectrometer. The echo was generated using a $\pi/2-\tau-\pi$ pulse sequence with 8 and 16 ns pulses, respectively. The echo intensity was integrated over a 48 ns window centered at the echo maximum. The delay between laser flash and initial microwave pulse was 400 ns. A Continuum Surelite Nd:YAG laser operating at 532 nm, 10 Hz, and 3.4 mJ/pulse was used to excite the sample.

Molecular Dynamics Modeling. Conformations of the protein side chains and cofactors were explored by restrained high-temperature molecular dynamics simulations for both wild type PS I and the PsaA-L722T mutant. Initial atomic coordinates for the wild type were taken from the 2.5 Å resolution crystal structure of PS I (PDB code: 1JB0).[6,7] All protein subunits, cofactors, lipids, and water molecules in the crystal structure were included in the model. Initial coordinates for the PsaA-L722T mutant were generated by virtual mutation of the residue PsaA-L722 to Thr using the Swiss-Pdb Viewer.[16] For both the wild type and the PsaA-L722T mutant, the AMBER program LEaP[17] was used to generate missing coordinates, including the positions of hydrogen atoms. A total of 20 sodium ions were added along the periphery of PS I to maintain electroneutrality. The NAMD scalable molecular dynamics package[18] using the all-atom AMBER-1994 force field[17,19] was used for all modeling of PS I interactions. AMBER parameters for chlorophyll, phylloquinone, and β-carotene cofactors were as derived from the ab initio force field developed by Ceccarelli et al.[20] and modified by Vasil'ev and Bruce.[21] The iron−sulfur clusters were considered to be in the oxidized state and their partial charges were determined from density functional theory calculations on $[Fe_4S_4(SCH_3)_4]^{2-}$.[22] Ideal bond lengths, angles, and dihedral angles for the iron−sulfur clusters were assumed to be those observed in the crystal structure.

A time step of 1 fs was used during molecular dynamics simulations. van der Waals interactions were smoothly reduced to zero using the standard X-PLOR switching function, between 10 Å and the cutoff radius of 13.0 Å. NAMD's multiple time-stepping scheme for full-electrostatic integration was employed, whereby the electrostatic interactions beyond

dx.doi.org/10.1021/jp309410w | J. Phys. Chem. B XXXX, XXX, XXX−XXX

the 13.0 Å cutoff were re-evaluated only every 4 time steps. The radius of the nonbonded neighbor list was set to 13.5 Å and neighbor lists were updated every 20 time steps. Covalent bonds to hydrogens were constrained using the SHAKE algorithm.[23]

The following protocol was used for molecular dynamics simulations of both wild type and PsaA-L722T PS I. The initial conformation was relieved of possible strain via conjugate gradient (CG) energy minimization for 2000 steps. The system was then heated to 300 K by reassigning the velocities of each atom and increasing the temperature by 0.001 K every time step over a total of 300 ps; no atom constraints were applied during this preliminary heating phase. Next, the system was heated from 300 K to 500 K over 200 ps, by velocity reassignment, during which only the cofactors, protein side chains, and the protein backbone between PsaA-N709 and PsaA-I724 were allowed to move. The positions of all other backbone atoms, solvent atoms, and Na^+ ions were held fixed. During a subsequent 200 ps equilibration period at 500 K, molecular conformations were saved every 100 time steps. This high temperature simulation was performed to enable the unrestrained components of the model to overcome energetic barriers and, thus, sample conformational space more broadly. Finally, every fifth conformation along the 2000 conformer trajectory at 500 K was selected for analysis; each was subjected to CG energy minimization until the root-mean-square gradient of the potential energy was <0.08 kcal/(mol Å). The positional constraints on backbone and solvent atoms and Na^+ ions were retained during the energy minimization. This procedure resulted in a total of 100 quenched (energy minimized) conformations for each form of PS I.

To assess possible artifacts introduced by the molecular mechanics forcefield and simulation protocol, the structures obtained from the simulation of wild type PS I were compared to the X-ray structure. The initial heating phase of the molecular dynamics simulation to 300 K caused a slight expansion of the protein backbone, but the root-mean-squared differences between the backbone (N, Cα, C, O) conformation of the X-ray structure and the models of the wild type and PsaA-L722T are both 0.8 Å over all 12 protein subunits and 0.7 Å over PsaA only. The H-bond between O4 of phylloquinone A and the backbone nitrogen of PsaA-L722 increases slightly in length from 2.69 Å in the X-ray structure to an average of 2.92 Å in the simulation, while the angle between the quinone C═O bond and the H-bond is unchanged at 159°.

QUANTUM CHEMICAL CALCULATIONS

The spin density distribution on the phylloquinone headgroup in the PsaA-L722T mutant was calculated using ONIOM type[24] QM:MM calculations (ONIOM is an acronym for our own N-layered integrated molecular orbital + molecular mechanics package. QM = quantum mechanical, MM = molecular mechanics). Structural models used in the ONIOM calculations were constructed starting from the model of Canfield et al.,[25] who used density functional theory (DFT) to refine the original PS I X-ray structure. Swiss-Pdb viewer[26] was used to change residue PsaA-722 from leucine to threonine. Two-layer ONIOM calculations ONIOM(B3LYP/6-31G+(d):Amber) were performed using Gaussian03.[27] The QM layer contained the headgroup and the first 4 carbon atoms of the phytyl tail of phylloquinone in the PsaA binding site. The remaining atoms of the protein residues formed the MM layer. Linking between the QM and MM layers was achieved using hydrogen link atoms. For the MM part of the calculation, the all-atom AMBER-1994 force field was used for the protein. For the cofactors an ab initio force field developed for the cofactors of bacterial photosynthetic reaction centers, which was parametrized to reproduce density functional theory vibrational modes, was used. All atoms of the cofactors, solvent and protein side chains, as well as the atoms of the protein backbone between PsaA-I717and PsaA-L736, were unconstrained during optimization.

RESULTS AND DISCUSSION

Transient EPR Spectra. Figure 2 shows room temperature transient EPR (TREPR) spectra and transients of PS I for wild type and the PsaA-L722T mutant. The arrows under the spectra indicate the magnetic field positions at which the transients were taken. At room temperature, the transient EPR spectra of both samples evolve from the *E*/*A*/*E* (*E* = emission, *A* = absorption) pattern of $P_{700}^+PhQ_A^-$ at early time to a predominantly emissive spectrum from $P_{700}^+F_X^-$ at late time. The spectra shown in Figure 2 have been extracted from the full data set by a kinetic fitting procedure described in the literature.[28] Representative transients are displayed in the bottom of Figure 2 to show the quality of the fit. ET in the B-branch of PS I is too fast to be resolved kinetically by TREPR, however, it is observed as a fraction of the emissive signal

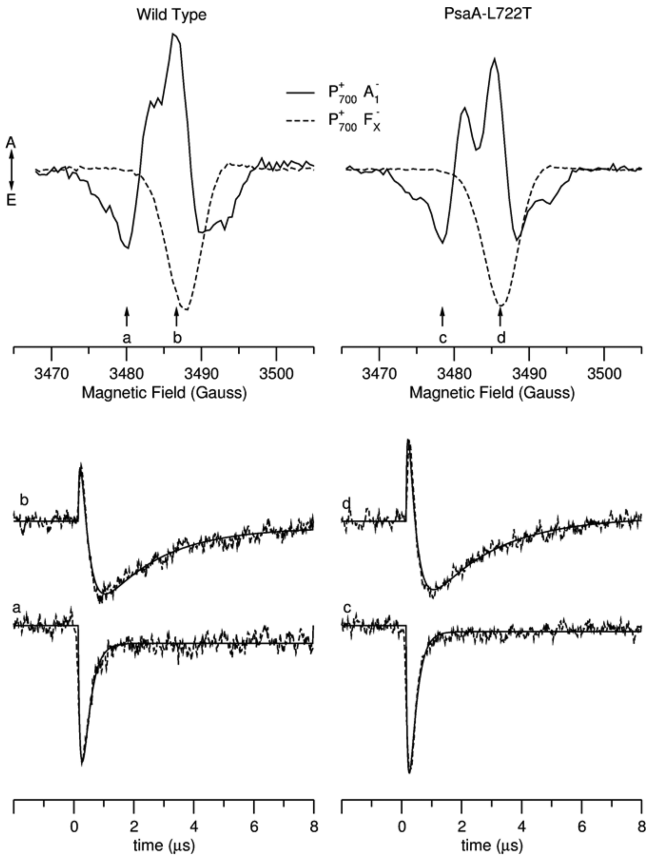

Figure 2. Room temperature transient EPR spectra and transients of PS I from the wild type and PsaA-L722T mutant strains of *Chlamydomonas rheinhardtii*. The spectra of $P_{700}^+PhQ^-$ and $P_{700}^+F_X^-$ have been extracted from the full data sets by kinetic fitting.[28] The transients yield lifetimes of 260 ± 30 and 200 ± 30 ns for $P_{700}^+PhQ_A^-$ in the wild type and Psa-L722T mutant, respectively.

dx.doi.org/10.1021/jp309410w | J. Phys. Chem. B XXXX, XXX, XXX−XXX

present at an earlier time. The size of this fraction can be determined approximately by fitting the data.[29] The fits yield lifetimes of 260 ± 30 ns and 200 ± 30 ns for forward ET from PhQ_A to F_X and amplitude ratios of 35:65 and 45:55 for the fast/slow phases of ET in the wild type and PsaA-L722T mutant, respectively. These values are consistent with the corresponding lifetimes of 256 ± 12 and 171 ± 10 ns and amplitude ratios of 37:63 and 49:51 obtained previously by optical methods.[12]

In Figure 2, the spectra of $P_{700}^+PhQ^-$ in the wild type and the PsaA-L722T mutant are noticeably different with a clear splitting of the central absorptive peak visible in the spectrum of the PsaA-L722T mutant, while the wild type shows only a shoulder. These differences are seen more clearly in the X- and Q-band spectra measured at 80 K, which are shown in Figure 3.

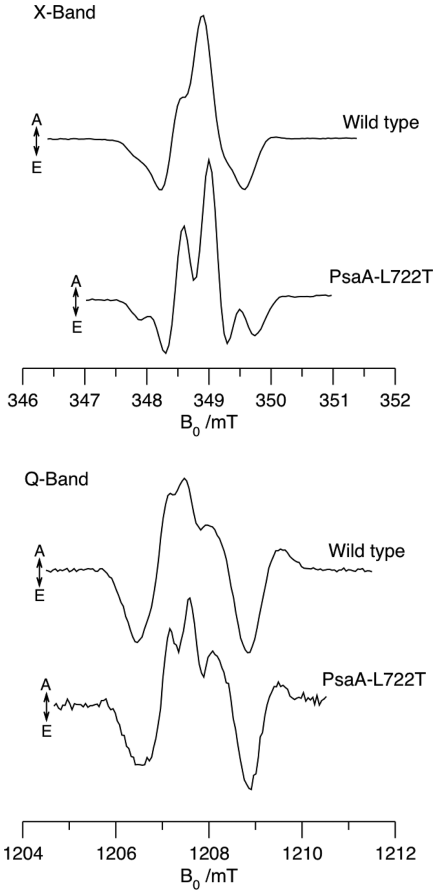

Figure 3. X- and Q-band TREPR spectra taken at 80 K. The spectra are the average signal intensity in a 400 ns wide time window centered at 850 ns after the laser flash.

At X-band (Figure 3, top), the spectrum of the PsaA-L722T mutant shows clear splitting of the downfield emission, the central absorption, and the upfield emission. At Q-band (Figure 3, bottom), the central absorption of the wild type has two shoulders that are known to arise from strong methyl hyperfine coupling on the *y*-component of the quinone **g**-tensor. In the corresponding spectrum of the PsaA-L722T mutant, these features are more pronounced. In contrast, the upfield region of the Q-band spectra, which arises primarily from transitions associated with P_{700}^+, is virtually identical in the wild type and the mutant. Thus, the change from Leu to Thr at residue PsaA-722 appears to cause an increase in the methyl hyperfine coupling of PhQ_A^-. In the wild type, the methyl hyperfine coupling is known to be large because of the asymmetry in the H-bonding. The single H-bond to the backbone N of PsaA-L722 distorts the spin density distribution in an alternating pattern around the quinone ring such that it is increased on the ring carbon adjacent to the methyl group.[30−32] The increased hyperfine coupling in the PsaA-L722T mutant implies that the spin density adjacent to the methyl group is further increased as a result of the mutation, which suggests even greater asymmetry in the H-bonding. Such a change in the H-bonding would be expected to lead to a more positive midpoint potential for PhQ_A in the PsaA-L722T mutant compared to the wild type because stronger H-bonding should stabilize the semiquinone. Such a change in midpoint potential should slow forward ET, which is opposite to the observed increase in the rate of forward ET in the PsaA-L722T mutant. However, the ET rate is also determined by the electronic coupling and by the reorganization energy.

Out-of-Phase Echo Modulation. It is possible that the electronic coupling between PhQ_A and F_X is altered in the PsaA-L722T mutant as a result of a change in the position of the quinone. This possibility can be explored using out-of-phase electron spin echo modulation measurements. The modulation curves depend strongly on the spin−spin coupling in the radical pair $P_{700}^+PhQ_A^-$ and, hence, on the distance between P_{700} and PhQ_A. If the position of the quinone is altered in the mutant, a change in the frequency in the echo modulation curve is expected. Experimental echo modulation curves for the wild type and PsaA-L722T mutant are compared in Figure 4. The

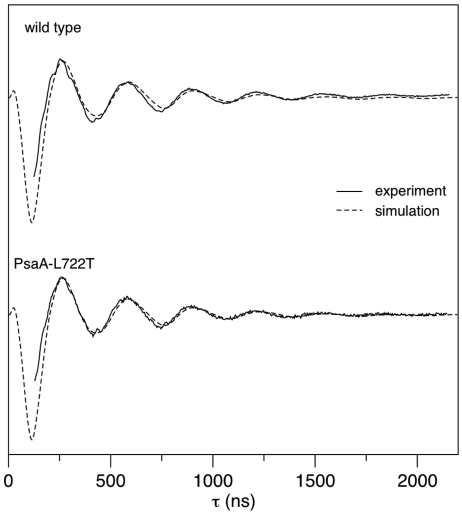

Figure 4. X-band out-of-phase electron spin echo envelope modulation curves of PS I from the wild type and PsaA-L722T mutant at 80 K. The dashed curves are calculated by integrating eq 1 of ref 33 over a random distribution of molecular orientations. The dipolar and exchange coupling constants in the simulation were set to $D = -170$ μT and $J = 1$ μT, as determined previously.[36,37].

dashed curves in the figure are calculated as described in refs 33−35 using the exchange and dipolar coupling constants determined previously.[36,37] As can be seen in Figure 4, the echo modulation curve from the PsaA-L722T mutant is essentially identical to that from the wild type and is reproduced well using the known coupling constants. Hence, we can conclude that the coupling and the distance between P_{700} and PhQ_A is not altered

dx.doi.org/10.1021/jp309410w | J. Phys. Chem. B XXXX, XXX, XXX−XXX

in the PsaA-L722T mutant, which implies that the position of PhQ_A does not change significantly.

However, the observed change in the ET lifetime, 260 ns for the wild type versus 200 ns for the PsaA-L722T mutant, is not large and so we need to consider whether the change in the distance between PhQ_A and F_X needed to account for it would lead to a measurable change in the echo modulation curves. Dutton's ruler[38] predicts that a decrease of 0.2 Å in the edge-to-edge distance between PhQ_A to F_X would account for the observed change in rate if all other factors remained the same. If PhQ_A were to move 0.2 Å closer to F_X along the vector joining the center of the PhQ_A headgroup and the center of F_X, the resulting change in the distance between P_{700} and PhQ_A is only 0.03 Å. This is about a factor of 5−10 smaller than is detectable in the echo modulation curves. Thus, we cannot discount the possibility that a change in the electronic coupling between F_X and PhQ_A resulting from a small change in the distance between them could contribute to the change in ET rate.

Molecular Dynamics Simulations. To investigate the structural changes in the phylloquinone binding pocket that cause the altered spin density distribution, we have performed molecular dynamics simulations of the mutant. The simulations probe the conformation space of each structure and yield families of conformers that represent local minima on the energy surface. Our primary interest is in the nature of the hydrogen bonding of the quinone. Figure 5 shows histograms of the distance between oxygen O_4 of PhQ_A and possible H-bond donors. The top histogram is for the wild type and shows the distance to the backbone N of PsaA-L722. The structure expands slightly during the initial heating phase of simulation, and as a result, the O−N distance for the wild type is ∼0.2 Å longer than observed in the crystal structure. As expected, a very narrow distribution of possible distances is found for the wild type and the average C−O−N angle of 160° in the simulation is identical to the value in the X-ray structure. In contrast to the wild type, the corresponding distribution of possible O−N distances in the PsaA-L722T mutant (Figure 5, middle) is much broader, and the entire distribution is shifted to considerably longer distances. Thus, the simulations show that when a wide conformation space is sampled by heating the system to 500 K, many conformers are found in which the H-bond between the oxygen O_4 of phylloquinone A and the backbone nitrogen is broken or weakened. This implies that there may be greater flexibility of the backbone.

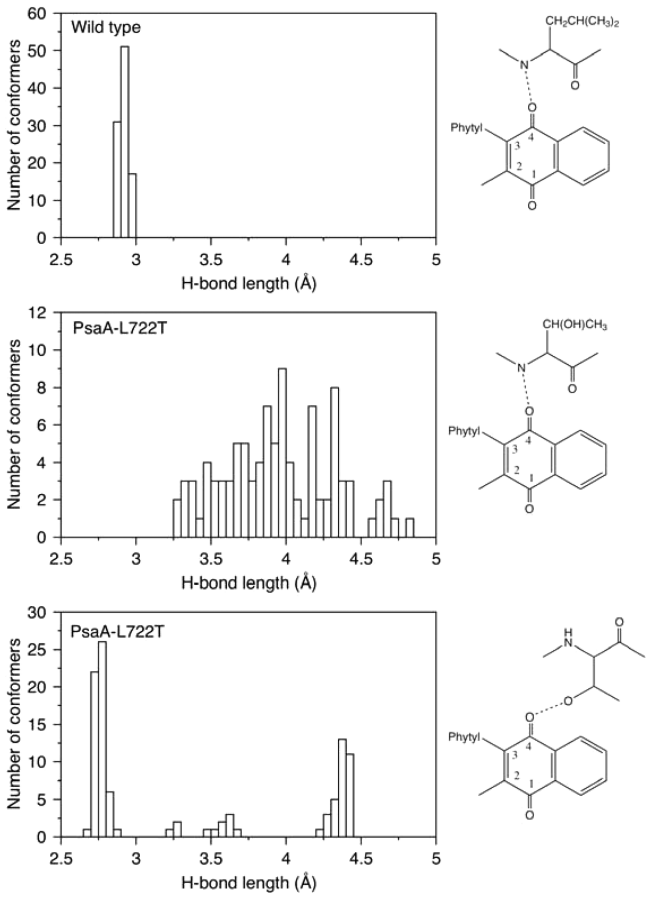

Figure 5. Histograms of possible H-bond distances from molecular dynamics simulations of PS I.

The finding that the H-bond to the backbone N may be disrupted in the PsaA-L722T mutant suggests that if the increased hyperfine splitting is due to stronger H-bonding, there should be an additional H-bond donor available to bind to O_4. The obvious candidate is the OH group of the Thr side chain. In the bottom panel of Figure 5, the distribution of distances between oygen O_4 of the phylloquinone and oxygen $O_{\gamma 1}$ of the Thr side chain is shown. As can be seen, the largest group of conformers is clustered around a distance of 2.8 Å, which is slightly shorter than the O−N distance obtained for the wild type. In addition, however, there are two smaller groups of conformers in which the O−O distances are ∼4.4 and ∼3.5 Å. Examples of the structures of the conformers with O−O distances of 2.8 and 4.4 Å are shown in Figure 6A and B, respectively.

A comparison of the two structures in Figure 6 shows that they correspond to two different rotomeric conformers of the threonine side chain about $C_\alpha-C_\beta$. In the conformer shown in Figure 6A (conformer 1), the side chain of PsaA-T722 is rotated such that the C−O bond of the OH group is directed toward the carbonyl group of the quinone. In the conformer in Figure 6B (conformer 3), the longer O−O distance of 4.8 Å arises from a rotation of the Thr side chain so that the C−O bond is directed away from the quinone. The intermediate O−O distances occur in the third rotomeric conformation of the side chain, which we refer to as conformer 2. From Figures 5 and 6, it is clear that the simulation predicts that a large number of low energy conformers exist in which the OH group of the Thr side chain is within H-bonding distance of oxygen O_4 of phylloquinone.

An important factor for the effect of the H-bond on the properties of the quinone is its direction with respect to the lone pairs on the carbonyl oxygen. In the X-ray structure of cyanobacterial PS I,[6,7] the C−O−N angle associated with the H-bond between phylloquinone A and the backbone of PsaA-L722 is 159° and the O−N direction is approximately 20° out of the quinone plane. For a linear H-bond along the long pair direction, these two angles would be 120 and 0°, respectively. However, a survey of a large number of organic crystals[39] shows that, although H-bonding along the lone pair direction is somewhat preferred, a wide range of geometries occur in nature and the H-bond arrangement found for PhQ_A in PS I is near the median of this distribution. A very different arrangement is found for the putative H-bond between the OH group of the Thr side chain and phylloquinone A in the PsaA-L722T mutant. For those conformers in which the $O_4-O_{\gamma 1}$ distance is less than 3 Å, the simulation gives an average $C_4-O_4-O_{\gamma 1}$ angle

dx.doi.org/10.1021/jp309410w | J. Phys. Chem. B XXXX, XXX, XXX−XXX

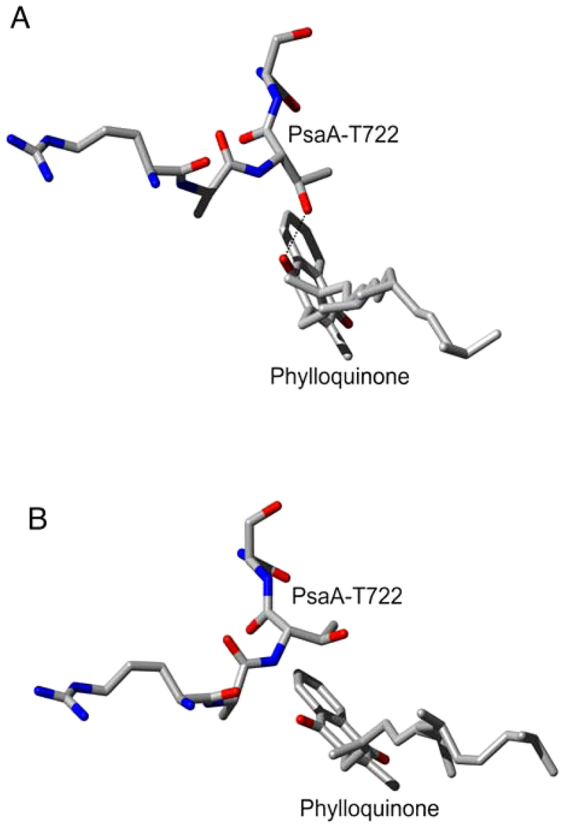

Figure 6. Representative conformers from the molecular dynamics simulation of the PsaA-L722T mutant: (A) conformer with a phylloquinone O_4 to Thr $O_{\gamma 1}$ O−O distance of 2.8 Å; (B) conformer with an O−O distance of 4.4 Å.

of 134° and an average angle between the O_4−$O_{\gamma 1}$ direction and the plane of the quinone carbonyl group of 65°. Because this geometry is very different from that of the H-bond in the wild type, its effect on the spin density distribution is not immediately apparent and quantum mechanical calculations are necessary.

QM/MM Calculations. The influence of the threonine side chain on the spin density distribution of phyllosemiquinone can be calculated using ONIOM type QM:MM methods. For phyllosemiquinone in the PsaA-L722T mutant, three separate calculations were performed, starting with the threonine side chain in each of the three possible conformations that are outlined in Figure 5C, with Oγ···O bond distances of ~2.75, 3.6, and 4.4 Å for conformers 1, 2 and 3, respectively.

The three models (for phyllosemiquinone in the PsaA-L722T mutant) were geometry optimized using the ONIOM-(B3LYP/6-31G+(d):AMBER) approach, and Table 1 lists calculated interatomic distances and angles between the A-branch phyllosemiquinone oxygen atoms and their surroundings. For comparison, Table 1 also lists ONIOM calculated geometry optimized data for phyllosemiquinone in WT PS I, as well as the corresponding distances and angles derived from the DFT refined structure model of Canfield et al.[25] for neutral phylloquinone in WT PS I.

The distance between the hydrogen atom of the Thr hydroxyl side chain and the oxygen atom of the C_4═O group of phyllosemiquinone (Thr H_γ−O_4 distance) for conformer 1 is 1.80 Å. Such a distance is typical for a H-bond. In conformers 2

Table 1. Interatomic Distances and Angles Involving the Oxygen Atoms of Phyllosemiquinone in WT and the PsaA-L722T Mutant Obtained from ONIOM Calculations[a]

	wild type		PsaA-L722T		
			conformer		
	DFT model[25]	ONIOM	1	2	3
	neutral	anion	anion	anion	anion
Thr $O_{\gamma 1}$−O_4			2.76	3.76	4.30
Thr H_γ−O_4			1.80	2.90	5.12
C_1═O	1.241	1.261	1.259	1.259	1.261
C_4═O	1.253	1.288	1.295	1.290	1.288
N−O_4	2.98	2.82	2.80	2.84	2.80
NH−O_4	1.95	1.82	1.79	1.84	1.81
∠N−H−O_4	170.7	164.7	171.1	165.8	162.8

[a]Distances are in Å and angles are in degrees.

and 3, the Thr H_γ−O_4 distance is 2.90 and 5.12 Å, both of which are well outside H-bonding distance.

In the X-ray structure and the ONIOM calculated models, the phylloquinone carbonyl bond-lengths reflect the asymmetric H-bonding environment, and the C_4═O bond (which is H-bonded) is longer than the C_1═O bond (which is not H-bonded). For neutral phylloquinone in WT PS I, the C_1═O and C_4═O bond lengths are 1.241 and 1.253 Å, respectively. For phyllosemiquinone in WT PS I ONIOM calculations indicate C_1═O and C_4═O bond lengths of 1.261 and 1.288 Å, respectively. As expected, phylloquinone reduction leads to a lengthening of both carbonyl bonds. The difference in their bond lengths also increases compared to the neutral state (0.027 vs 0.008 Å). For phyllosemiquinone in the PsaA-L722T mutant, the C_4═O bond is lengthened to 1.295 Å in conformer 1 (1.288 Å in WT), possibly indicating stronger/additional H-bonding to the Thr hydroxyl group.

The ONIOM models indicate that the distance between the backbone nitrogen of residue PsaA722 and the C_4═O oxygen atom of phyllosemiquinone is roughly the same in the wild type and the PsaA-L722T mutant. This result differs from that found with the MD simulations (Figure 5B) because of the different approaches taken for the two types of calculations. In the MD simulations, the system is heated to 500 K to ensure that as wide a range of conformers as possible are sampled. However, in the ONIOM calculations for PsaA722 the temperature is kept at 300 K and a narrower range of backbone conformations is sampled.

Table 2 shows the methyl hyperfine coupling tensors of phyllosemiquinone calculated for the wild type and the three conformers of the PsaA-L722T mutant. Experimental and calculated values for the wild type are from Niklas et al.[40] The ONIOM model of the wild type reproduces the DFT values very well, apart from a slightly different orientation of the tensor axes. For conformer 1 of the PsaA-L722T mutant, both the isotropic hyperfine coupling and the anisotropy of the tensor increase as a result of the additional H-bond. In conformer 2, the coupling and anisotropy are also increased compared to the wild type, but less so than in conformer 1. The coupling and anisotropy for conformer 3 is essentially the same as for the wild type. To examine the effect of these changes on the methyl hyperfine coupling, we have calculated the spin polarized EPR spectra of $P_{700}{}^{+}PhQ_A{}^{-}$ using the known parameters[41] for native PS I in *T. elongatus* and replacing the wild type hyperfine coupling tensor with those calculated for

dx.doi.org/10.1021/jp309410w | J. Phys. Chem. B XXXX, XXX, XXX−XXX

Table 2. Principal Values and Orientation of the 2-Methyl Hyperfine Coupling Tensor of Phylloquinone A in PS I[a]

	wild type			PsaA-L722T		
				conformer		
	experiment[40,b]	DFT[40]	ONIOM model	1	2	3
A_{xx}	8.8 (9.1)	9.62	9.0	10.4	10.6	9.0
A_{yy}	12.4 (12.7)	13.05	13.0	15.0	13.3	13.2
A_{zz}	8.3 (8.6)	8.86	9.2	10.6	10.8	8.9
a_{iso}	9.8 (10.1)	10.51	10.4	12.0	11.6	10.4
θ^c	0	1	13	−2.2	2.2	6
ϕ^c	30	14	17	15	17	15

[a]The coupling constants are given in MHz and the angles are in degrees. [b]The experimental coupling constants are taken from the literature[40] and were measured for the state $P_{700}^{+}PhQ_A^{-}$ in PS I from *T. elongatus*. The values in parentheses are for the photoaccumulated phyllosemiquinone in the same samples. [c]A clockwise rotation about the *y*-axis by θ followed by a clockwise rotation by ϕ about the *z*-axis transforms the principal axes of the hyperfine tensor into those of the **g**-tensor.

the PsaA-L722T mutant (Table 2). As can be seen in Figure 7, the hyperfine coupling tensor computed for conformer 1

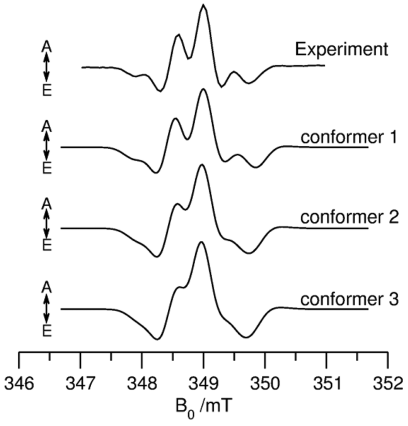

Figure 7. X-band TREPR spectra of $P_{700}^{+}PhQ_A^{-}$ in the PsaA-L722T mutant. In the calculated spectra, the known parameters[41] for the wild type have been used with the methyl hyperfine coupling tensor given by the ONIOM QM/MM calculations shown in Table 2.

reproduces the experimental spectrum very well. Thus, the observed splitting is consistent with the formation of a H-bond between the Thr side chain and oxygen O_4 of phylloquinone PhQ_A and retention of the H-bond to the backbone nitrogen.

Electron Transfer Energetics. The faster rate of ET at room temperature for the PsaA-L722T mutant implies that the activation energy for A-branch ET is lowered as a result of the mutation. On the other hand, the H-bonding to the Thr side chain is expected to stabilize the charge on the semiquinone, which would lead to an increase in the activation energy if the reorganization energy remains the same. The mutation might also be expected to influence the electronic coupling and the frequency of the modes coupled to the ET. To investigate these effects, we have measured the temperature dependence of the rate of A-branch ET in the PsaA-L722T mutant. The rates were obtained from TREPR traces as described for the room temperature data above.

The measured rates are shown as an Arrhenius plot in Figure 8 along with data from the literature for the two phases in the

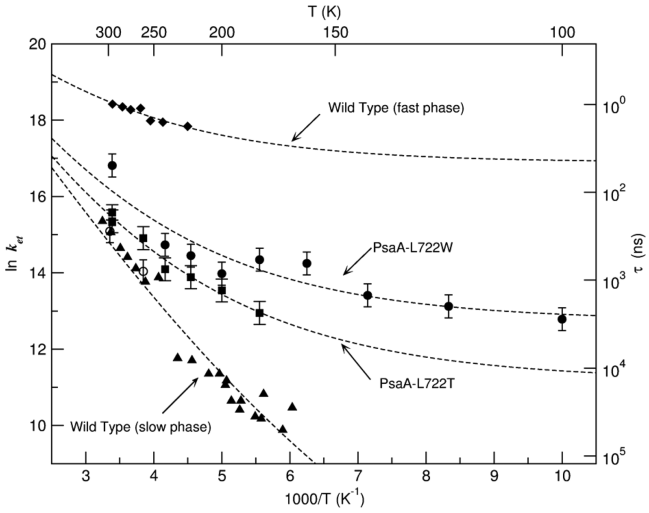

Figure 8. Temperature dependence of the rate of ET from phylloquinone to F_X: squares, PsaA-L722T, EPR data (this work); closed circles, PsaA-L722W, EPR data from ref 11; open circles, wild type slow phase, EPR data from ref 11; triangles, wild type slow phase, optical data from ref 42; diamonds, wild type fast phase, optical data from ref 43. The dashed curves are fits of the data using the semiclassical approach developed by Hopfield.[44] The parameters used are discussed in the text.

wild type[42,43] and the PsaA-L722W mutant.[11] As can be seen in Figure 8, the difference between the ET rate in the PsaA-L722T mutant (squares) and the slow phase in the wild type (diamonds) becomes quite large as the temperature is decreased such that they differ by roughly a factor of 10 at 200 K. In contrast to this difference, the temperature dependences of the rates for the PsaA-L722T mutant and the PsaA-L722W mutant are roughly parallel. The fast phase of the wild type is also included in the plot for comparison. To identify possible origins for the different temperature dependences of the different samples we have fit the data using the semiclassical Marcus equation derived by Hopfield:[44]

$$k = \frac{2\pi|V|^2}{\hbar\sqrt{2\pi\sigma^2(T)}}\exp\{-(\Delta G + \lambda)^2/2\sigma^2(T)\} \quad (1)$$

where $\sigma^2(T) = \hbar\omega\lambda\coth(\hbar\omega/2k_BT)$ is the Gaussian width of the vibrational potential energy surface associated with the ET and ω is the frequency of the vibrational mode. To fit eq 1, to the data in Figure 8, the reorganization energy, λ, the electronic coupling $|V|^2$, the activation energy $(\Delta G + \lambda)^2/4\lambda k_B$ and the frequency of the vibrational mode, ω, must be determined. If all four of these parameters are varied simultaneously, it is not possible to obtain physically reasonable values for the reorganization energy. Hence, we have chosen to keep it constant at the common value λ = 700 meV found for the ET reactions in purple bacterial reaction centers[45] and only the activation energy, electronic coupling, and the frequency of the vibrational mode were varied in the fits. The values obtained for these three quantities are summarized in Table 3. For the PsaA-L722T mutant the activation energy is found to be about 10 meV higher than in the wild type (255 vs 243 meV), whereas for the PsaA-L722W mutant the activation energy is 10 meV lower than in the wild type. These values suggest that the stabilization of the charge from the additional H-bond between PhQ_A and the threonine side chain is roughly the same as the destabilization in PsaA-L722W due to disruption of the H-bond

dx.doi.org/10.1021/jp309410w | J. Phys. Chem. B XXXX, XXX, XXX−XXX

Table 3. Thermodynamic Parameters Obtained by Fitting Eq 1 to the Electron Transfer Rates Shown in Figure 8

sample	activation energy[a] (meV)	electronic coupling[b] (meV^2)	vibrational mode frequency (cm^{-1})
wild type (slow phase)	243	1.04	173
wild type (fast phase)	147	0.54	378
PsaA-L722T	255	1.25	320
PsaA-L722W	233	1.04[c]	325

[a]The activation energy is given by $(\Delta G + \lambda)^2/4\lambda k_B$. [b]The reorganization energy, λ, has been kept fixed at 700 meV. The electronic coupling is $|V|^2$ in eq 1. [c]Held fixed in the fit.

to the protein backbone. From the activation energies, we estimate that each of the H-bonds contributes ~25 meV to the stabilization of the charge. The fits also indicate that the higher ET rate in the PsaA-L722T mutant compared to the wild type is due to a slight increase in the electronic coupling from 1.04 meV^2 in the wild type to 1.25 meV^2. In contrast to these relatively small changes in the activation energy and electronic coupling, the frequencies of the vibrational modes differ significantly in the wild type versus in the PsaA-L722T mutant (173 and 320 cm^{-1}, respectively). The vibrational frequencies obtained for the two mutants PsaA-L722T and PsaA-L722W are almost the same (320 and 325 cm^{-1}, respectively), and the activation energy is slightly lower in the PsaA-L722W mutant (233 vs 255 meV in the PsaA-L722T mutant). For the fast phase of the wild type, the activation energy is significantly lower (147 meV) and the frequency is much higher (378 cm^{-1}). Thus, there are two main outcomes of these fits. First, they show that both the electronic coupling and the activation energy need to be considered when interpreting small mutation-induced changes in the ET rates. Second, the values for the frequency of the mode that couples to the ET differ strongly between the kinetic phases of the wild type and between the slow phase in the mutants and in the wild type. In the Hopfield model, the frequency describes the zero point energy and models the transition from classical Arrhenius behavior to quantum mechanical behavior as the temperature is lowered. Importantly, the model does not take coupling of the ET kinetics to the surroundings into account and it is likely that the change in slope in the experimental data reflects the dynamic arrest of the protein at the glass transition temperature ~200 K rather than quantum mechanical effects.

For the PhQ to F_X ET step, the rate is in the range of 10^8–10^6 s^{-1}. Thus, above the protein glass transition temperature at ~200 K,[46−48] the dynamic relaxation lifetime, τ_R, of the surrounding protein is expected to be shorter than the ET lifetime (τ_{ET}), but below this temperature we have $\tau_{ET} \gg \tau_R$. If the ET is coupled to the relaxation of the protein, a change in the slope of the Arrhenius plot is expected at the glass transition temperature. Such behavior is well-known in artificial photosynthetic systems[49] near solvent phase transitions and accounts for their dramatically altered electron transfer kinetics observed in the nematic phase of liquid crystalline solvents. Recently, a description of the temperature dependence near the glass transition temperature that takes the freezing out of the protein relaxation into account has been proposed[50] and from molecular dynamics simulations, it has been suggested that it can lead to a temperature-independent ET rate below the glass transition temperature.[51,52] The transition from activated to activationless ET occurs when modes of the protein coupled to ET become slower than the ET rate. The data in Figure 8 suggest that for the PhQ to F_X ET step, freezing out of the protein motion may lead to temperature-independent ET at the rate reached at the glass transition temperature.

CONCLUSIONS

The EPR data and calculations presented here strongly suggest that in the PsaA-L722T mutant an H-bond is formed between the phylloquinone O_4 and the Thr side chain OH group. If the reorganization energy is assumed to remain constant at 700 meV, we estimate that the change in the H-bonding raises the reduction midpoint potential of the quinone by ~20 meV, which results in an increase of ~10 meV in the activation energy. However, the higher activation barrier appears to be offset by slightly stronger electronic coupling between PhQ_A to F_X and, as a result, a small increase in the rate occurs. The deviations from linearity of the Arrhenius plots of the PhQ_A to F_X electron tranfer in the PsaA-L722T and PsaA-L722W mutants near the protein glass transition temperature is a strong indication that protein relaxation plays an important role in determining the rate of this step.

AUTHOR INFORMATION

Corresponding Author

*E-mail: avde@brocku.ca; kevin.redding@asu.edu.

Notes

The authors declare no competing financial interest.

ACKNOWLEDGMENTS

This work was support by Discovery Grants from the Natural Sciences and Engineering Research Council, Canada, to A.v.d.E. and H.G. and by the Division of Chemical Sciences, Geosciences, and Biosciences, Office of Basic Energy Sciences of the U.S. Department of Energy through Grant DE-FG02-08ER15989 to K.E.R. N.Z. acknowledges support from the Molecular Basis of Disease program at Georgia State University and G.H. acknowledges support from the Qatar National Research Fund, Award No. NPRP 4-183-1-034.

REFERENCES

(1) *Photosystem I, The Light-Driven Plastocyanin:Ferredoxin Oxidoreductase*; Golbeck, J. H., Ed.; Springer: Dordrecht, The Netherlands, 2006; Vol. *24*.

(2) Redding, K.; van der Est, A. Directionality of Electron Transfer in Photosystem I. In *Phototosystem I: The Light-Induced Plastocyanin:Ferredoxin Oxidoreductase*; Golbeck, J., Ed.; Springer: Dordrecht, 2006; Vol. *25*; pp 413−437.

(3) Ozawa, S. I.; Kosugi, M.; Kashino, Y.; Sugimura, T.; Takahashi, Y. *Plant Cell Physiol.* **2012**, *53*, 237−243.

(4) Ishikita, H.; Knapp, E. W. *J. Biol. Chem.* **2003**, *278*, 52002−52011.

(5) Prince, R. C.; Dutton, P. L.; Bruce, J. M. *FEBS Lett.* **1983**, *160*, 273−276.

(6) Fromme, P.; Jordan, P.; Krauß, N. *Biochim. Biophys. Acta* **2001**, *1507*, 5−31.

(7) Jordan, P.; Fromme, P.; Witt, H. T.; Klukas, O.; Saenger, W.; Krauß, N. *Nature* **2001**, *411*, 909−917.

(8) Koradi, R.; Billeter, M.; Wüthrich, K. *J. Mol. Graph.* **1996**, *14*, 51−55.

(9) Srinivasan, N.; Chatterjee, R.; Milikisiyants, S.; Golbeck, J. H.; Lakshmi, K. V. *Biochemistry* **2011**, *50*, 3495−3501.

(10) Srinivasan, N.; Karyagina, I.; Bittl, R.; van der Est, A.; Golbeck, J. H. *Biochemistry* **2009**, *48*, 3315−3324.

(11) Srinivasan, N.; Santabarbara, S.; Rappaport, F.; Carbonera, D.; Redding, K.; van der Est, A.; Golbeck, J. H. *J. Phys. Chem. B* **2011**, *115*, 1751−1759.
(12) Santabarbara, S.; Reifschneider, K.; Jasaitis, A.; Gu, F. F.; Agostini, G.; Carbonera, D.; Rappaport, F.; Redding, K. E. *J. Phys. Chem. B* **2010**, *114*, 9300−9312.
(13) Li, Y.; Lucas, M. G.; Konovalova, T.; Abbott, B.; MacMillan, F.; Petrenko, A.; Sivakumar, V.; Wang, R.; Hastings, G.; Gu, F.; et al. *Biochemistry* **2004**, *43*, 12634−12647.
(14) Picard, V.; Ersdal-Badju, E.; Lu, A.; Bock, S. C. *Nucleic Acids Res.* **1994**, *22*, 2587−2591.
(15) Subramanyam, R.; Jolley, C.; Brune, D. C.; Fromme, P.; Webber, A. N. *FEBS Lett.* **2006**, *580*, 233−238.
(16) Guex, N.; Peitsch, M. C. *Electrophoresis* **1997**, *18*, 2714−2723.
(17) Case, D. A.; Darden, T. A.; Cheatham, T. E.; Simmerling, C. L.; Wang, J.; Duke, R. E.; Luo, K. M.; Merz, K. M.; Wang, B.; Perlman, D. A.; et al. *AMBER 8*; University of California: San Francisco, 2004.
(18) Phillips, J. C.; Braun, R.; Wang, W.; Gumbart, J.; Tajkhorshid, E.; Villa, E.; Chipot, C.; Skeel, R. D.; Kale, L.; Schulten, K. *J. Comput. Chem.* **2005**, *26*, 1781−1802.
(19) Cornell, W. D.; Cieplak, P.; Bayly, C. I.; Gould, I. R.; Merz, J., K. M.; Ferguson, D. M.; Spellmeyer, D. C.; Fox, T.; Caldwell, J. W.; Kollman, P. A. *J. Am. Chem. Soc.* **1994**, *117*, 5179−5197.
(20) Ceccarelli, M.; Procacci, P.; Marchi, M. *J. Comput. Chem.* **2003**, *24*, 129−142.
(21) Vasil'ev, S.; Bruce, D. *Biophys. J.* **2006**, *90*, 3062−3073.
(22) Mouesca, J.-M.; Chen, J. L.; Noodleman, L.; Bashford, D.; Case, D. A. *J. Am. Chem. Soc.* **1994**, *116*, 11898−11914.
(23) Ryckaert, J. P.; Ciccotti, G.; Berendsen, H. J. C. *J. Comput. Phys.* **1977**, *23*, 327−341.
(24) Dapprich, S.; Komaromi, I.; Byun, K. S.; Morokuma, K.; Frisch, M. J. *J. Mol. Struct.: THEOCHEM* **1999**, *461*, 1−21.
(25) Canfield, P.; Dahlbom, M. G.; Hush, N. S.; Reimers, J. R. *J. Chem. Phys.* **2006**, 124.
(26) Geux, N.; Peitsch, M. C. *Electrophoresis* **1997**, *18*, 2714−2723.
(27) Frisch, M. J.; Trucks, G. W.; Schlegel, H. B.; Scuseria, G. E.; Robb, M. A.; Cheeseman, J. R.; Montgomery, J. J. A.; Vreven, T.; Kudin, K. N.; Burant, J. C.; et al. *Gaussian 03*, revision D.01; Gaussian, Inc.: Wallingford, CT, 2004.
(28) van der Est, A.; Bock, C.; Golbeck, J.; Brettel, K.; Setif, P.; Stehlik, D. *Biochemistry* **1994**, *33*, 11789−11797.
(29) Li, Y. J.; van der Est, A.; Lucas, M. G.; Ramesh, V. M.; Gu, F. F.; Petrenko, A.; Lin, S.; Webber, A. N.; Rappaport, F.; Redding, K. *Proc. Natl. Acad. Sci. U.S.A.* **2006**, *103*, 2144−2149.
(30) Pushkar, Y. N.; Ayzatulin, O.; Stehlik, D. *Appl. Magn. Reson.* **2005**, *28*, 195−211.
(31) Pushkar, Y. N.; Golbeck, J. H.; Stehlik, D.; Zimmermann, H. *J. Phys. Chem. B* **2004**, *108*, 9439−9448.
(32) Pushkar, Y. N.; Stehlik, D.; van Gastel, M.; Lubitz, W. *J. Mol. Struct.* **2004**, *700*, 233−241.
(33) Bittl, R.; Zech, S. G. *Biochim. Biophys. Acta* **2001**, *1507*, 194−211.
(34) Tang, J.; Thurnauer, M. C.; Norris, J. R. *Chem. Phys. Lett.* **1994**, *219*, 283−290.
(35) Salikhov, K.; Kandrashkin, Y. E.; Salikhov, A. K. *Appl. Magn. Reson.* **1992**, *1*, 199−216.
(36) Zech, S. G.; Lubitz, W.; Bittl, R. *Ber. Bunsen-Ges.* **1996**, *100*, 2041−2044.
(37) Bittl, R.; Zech, S. G. *J. Phys. Chem. B* **1997**, *101*, 1429−1436.
(38) Moser, C. C.; Dutton, P. L. *Biochim. Biophys. Acta* **1992**, *1101*, 171−176.
(39) Taylor, R.; Kennard, O. *Acc. Chem. Res.* **1984**, *17*, 320−326.
(40) Niklas, J.; Epel, B.; Antonkine, M. L.; Sinnecker, S.; Pandelia, M. E.; Lubitz, W. *J. Phys. Chem. B* **2009**, *113*, 10367−10379.
(41) Kandrashkin, Y. E.; Vollmann, W.; Stehlik, D.; Salikhov, K.; van der Est, A. *Mol. Phys.* **2002**, *100*, 1431−1443.
(42) Schlodder, E.; Falkenberg, K.; Gergeleit, M.; Brettel, K. *Biochemistry* **1998**, *37*, 9466−9476.
(43) Agalarov, R.; Brettel, K. *Biochim. Biophys. Acta* **2003**, *1604*, 7−12.
(44) Hopfield, J. J. *Proc. Natl. Acad. Sci. U.S.A.* **1974**, *71*, 3640−3644.
(45) Moser, C. C.; Keske, J. M.; Warncke, K.; Farid, R. S.; Dutton, P. L. *Nature* **1992**, *355*, 796−802.
(46) Doster, W.; Cusack, S.; Petry, W. *Nature* **1989**, *337*, 754−756.
(47) Ferrand, M.; Dianoux, A. J.; Petry, W.; Zaccai, G. *Proc. Natl. Acad. Sci. U.S.A.* **1993**, *90*, 9668−9672.
(48) Rasmussen, B. F.; Stock, A. M.; Ringe, D.; Petsko, G. A. *Nature* **1992**, *357*, 423−424.
(49) Wiederrecht, G. P.; Svec, W. A.; Wasielewski, M. R. *J. Phys. Chem. B* **1999**, *103*, 1386−1389.
(50) Matyushov, D. V. *J. Chem. Phys.* **2005**, 122.
(51) LeBard, D. N.; Matyushov, D. V. *J. Chem. Phys.* **2008**, 128.
(52) Lebard, D. N.; Matyushov, D. V. *J. Phys. Chem. B* **2009**, *113*, 12424−12437.